Modeling a Carbonyl Group Taking into Account Back-Donation Effects through the Effective Group Potential Method

Fabienne Bessac, Fabienne Alary,* Romuald Poteau, Jean-Louis Heully, and Jean-Pierre Daudey

Laboratoire de Physique Quantique, UMR 5626 du CNRS, IRSAMC, Université Paul Sabatier, 118 route de Narbonne, F31062 Toulouse Cedex, France

Received: April 16, 2003; In Final Form: August 1, 2003

Quantum chemical calculations have been carried out at different levels of theory in order to verify the validity of an effective group pseudopotential (EGP) for carbonyl. Carbonyl potential groups are designed to reproduce the nature of the bonding between the carbonyl group and transition metal elements. This work is a part of a series of articles which investigate different bonding situations (Alary, F.; Poteau, R.; Heully, J.-L.; Barthelat, J.-C.; Daudey, J.-P. *Theor. Chem. Acc.* **2000**, *104*, 174−178; Poteau, R.; Ortega, I.; Alary, F.; Solis, A. R.; Barthelat, J.-C.; Daudey, J.-P. *J. Phys. Chem. A* **2001**, *105*, 198−205; Poteau, R.; Alary, F.; Makarim, H. A. E.; Heully, J.-L.; Barthelat, J.-C.; Daudey, J.-P. *J. Phys. Chem. A* **2001**, *105*, 206−214; Alary, F.; Heully, J.-L.; Poteau, R.; Maron, L.; Trinquier, G.; Daudey, J.-P. *J. Am. Chem. Soc.* **2003**, *125*, 11051−11061). The present contribution is the first attempt at modeling a chemical group involved in a donation−back-donation bond. Three pseudocarbonyl groups, extracted from different systems, are discussed here; two are produced from the isolated carbonyl molecule and the other from BH_3CO. Two uses are considered here. The transferability of such groups has to be proven by the reproduction of electronic and geometrical parameters of various molecules of interest: BF_3CO, $Co(PH_3)_2HCO$, $Ni(CO)_4$, or $Fe(CO)_5$ is a preliminary efficient test. The third of the aforementioned molecules, $Ni(CO)_4$, is further investigated. The EGP approach is questioned here when faced with the problem of excited state determination using several calculation methods: CASSCF/CASPT2 and TDDFT (TD-LDA).

I. Introduction

The spatial separability of certain functional groups in molecules allows us to divide chemical systems into subsystems, namely, active parts and inactive or spectator parts. According to the effective group pseudopotential (EGP) methodology, spectator groups can be replaced by a reduced pseudogroup. Modeling a carbonyl with the EGP method means first that it is replaced by a fictitious system, that is, a reduced number of nuclei and electrons and a truncated basis set, and second that the EGP operator spread out on the fictitious system restores the effect of a real carbonyl group. Just as the core pseudopotential method (ECP) implies spatial and energetic separabilities between the electrons included in the core pseudopotential and the other electrons of the atom, the group pseudopotential method depends on the spatial separability between the electrons contained in the group pseudopotential and the other electrons of the molecule. We have previously described the results of our investigations of different bonding situations.[1−4] Our purpose here is to model a carbonyl group with an EGP, but extracting a pseudocarbonyl is a challenge for our method. Indeed repolarization effects and metal−ligand donor−acceptor phenomena occurred frequently when dealing with transition metal (TM) complexes containing CO ligands. Thus, the carbonyl is not exactly a spectator group within TM complexes, because the spatial separability for carbonyl is not exactly fulfilled. Nevertheless, designing a pseudocarbonyl is interesting for two main reasons. First, even if the carbonyl is intrinsically not a bulky ligand, most of the time several of them are part of a single organometallic complexes such as in $Fe(CO)_5$. Second, until now all groups already modeled by EGPs interacted by their occupied orbitals such as NH_3 or Cp (cyclopentadienyl). Moreover, NH_3 interacts via its σ lone pair only and Cp via a π system only. In contrast, the carbonyl binds because of its last occupied molecular orbital (MO), which is the n_c lone pair and its lowest virtual π shell.

The carbonyl ligand is unsaturated by virtue of the C−O multiple bond. Its ability to accept metal d_π electrons by back-bonding makes it a powerful π acceptor ligand. Therefore, CO is an excellent ligand for stabilizing electron-rich low-valent metal centers such as Mn, Cr, Fe, Ni, and so forth. As a consequence, the highest occupied molecular orbital (HOMO) of the carbonyl is the carbon σ lone pair, and the virtual π^* orbitals are more strongly developed on the carbon atom (see Figure 1). Because the oxygen is more electronegative than the carbon, its atomic orbitals (AO) are lower in energy than those of the carbon. In organometallic molecules, the frontier orbitals of the metal and the ligand generally dominate the bonding; thus, the TM is bonded to the carbonyl through the carbon. The bond between the carbonyl and the metal to form TM complexes mainly involves the carbon lone pair 5σ and the $2\pi^*$ degenerate orbitals of the carbonyl. However, bonding in metal−CO adducts like carbon monoxide complexes of Cp_2M (M = Ca, Eu, or Yb) which is of current theoretical interest exhibits bonding by the oxygen atom.[5]

The most common bonding model (see Figure 2) describes the TM−CO bond within the frontier orbital theory, implying

* Corresponding author. Fax: (33) 561556065. E-mail: fabienne.alary@irsamc.ups-tlse.fr.

10.1021/jp035020c CCC: $25.00
Published on Web 10/10/2003

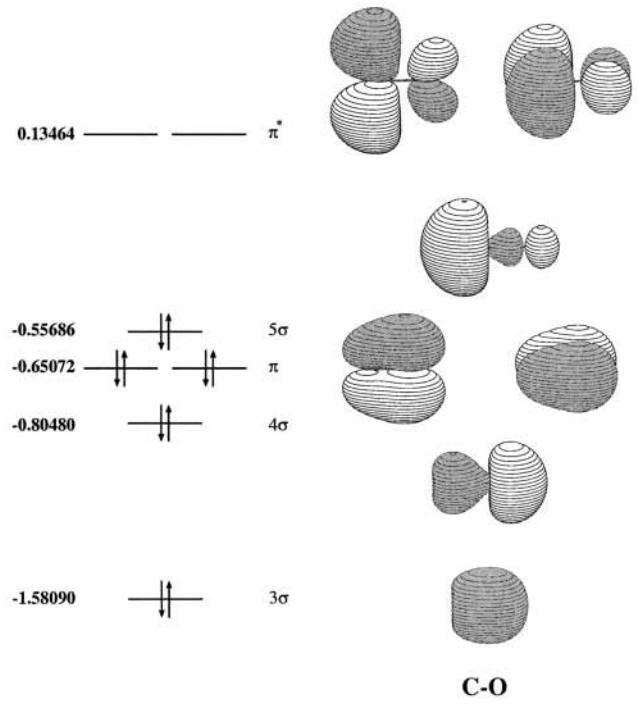

Figure 1. MO diagram of the carbonyl ligand; on the left, the orbital Hartree−Fock energies are shown in hartrees (Stuttgart ECP and basis sets for O and C).

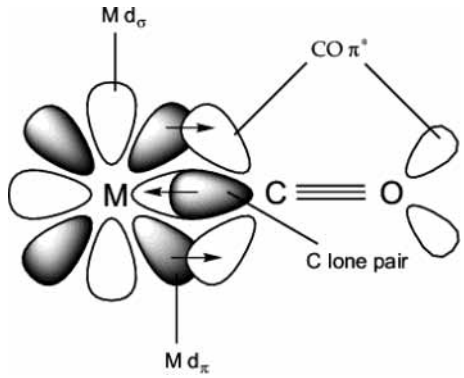

Figure 2. MO diagram representing CO π bonding.

a donation from the carbonyl 5σ orbital to the empty metal atomic orbitals of σ symmetry and a back-donation into the carbonyl 2π* orbitals from the occupied π-type d orbitals of the metal. When donation and back-donation concepts are included, the model is known as the Dewar−Chatt−Duncanson (DCD) model[6,7] in inorganic chemistry and the Blyholder model[8] in the area of adsorption of ligands on metallic surfaces.

Using the Energy Transition State (ETS)[9] analysis of iron pentacarbonyl, $Fe(CO)_5$, Uddin and Frenking[10] were able to get insight into the strength of the carbonyl ligand as a π acceptor. In such an analysis, the percentage contribution of the total orbital interactions (ΔE_{orb}) to the total attractive interactions reflects the covalent character of the bond. In given cases, symmetry arguments allow them to calculate the percentage contribution of the π or σ systems (ΔE_π, ΔE_σ) to ΔE_{orb}. Uddin and Frenking have shown that ΔE_{orb} represents 48.3% of the total attractive interactions for an axial carbonyl group and 45.3% for an equatorial carbonyl. ΔE_π is 47.9% of the total orbital interactions for axial carbonyls and 51.8% for equatorial carbonyls. It can be seen that the σ donation and π back-donation of the carbonyl group in TM complexes have similar strengths in the covalent part of the bonding.

With the constrained space orbital variation (CSOV) method of analysis , Bauschlicher and Bagus[11] have investigated TM−CO bondings in $Ni(CO)_4$ and $Fe(CO)_5$. Their conclusions differ slightly from those obtained by Uddin and Frenking. They have reached two main critical conclusions about the nature of TM−CO interactions. First, CSOV analysis exhibits an important σ repulsion between the two fragments, that is, the metal and the $(CO)_n$ cage. Second, the σ donation from CO to the 3d orbitals of the metal is greater for $Fe(CO)_5$ than for $Ni(CO)_4$. They explain this fact by considering the 3d shell of the metal. In $Fe(CO)_5$, Fe is d^8 and the $3d_{a1}$ orbital, which is involved in the σ donation from CO to Fe, is empty, whereas in $Ni(CO)_4$, Ni is d^{10} and the σ donation from CO to Ni is small. Moreover, the back-donation from the metal to CO is always important. Indeed, it is the only relevant charge-transfer contribution to the interaction for $Ni(CO)_4$, and its contribution to the interaction in $Ni(CO)_4$ is three times greater than that of the σ donation (CO → TM).

However, although the frontier orbital model has qualitatively explained many interactions, for the carbonyl ligand there have been indications that the electronic structure might not be fully explained by back-donation into the π* orbitals. Nyberg[12] studied the adsorption of both isoelectronic neutral ligands N_2 and CO onto metallic surfaces. Comparing theoretical data and results from X-ray spectroscopy, he showed that the π and σ interactions between the carbonyl ligand and TM are better described by a three-orbital interaction model (see Figure 3) than by the Blyholder model.

To obtain a satisfactory pseudocarbonyl, results from previous investigations involving carbonyls should be used when applying the EGP extraction method. The previous short and unexhaustive overview of different approaches used to gain insight into the carbonyl ligand shows that the question of the CO bonding mode with TMs has no easy and straightforward answers.

In this paper, we make a detailed description of the extraction process of an EGP group for carbonyl. In the following part, we summarize the important steps of the EGP method for the extraction of pseudogroups. In part III, we present and discuss some results which are of different types. First, geometry optimizations enable us to validate our pseudocarbonyls for various structural problems. Second, analysis of the electronic density for the TM complexes, $Fe(CO)_5$ and $Ni(CO)_4$, clarifies the behavior of our pseudocarbonyls bonded with TMs. Third, a study of the first low-lying singlet states excitation energies of $Ni(CO)_4$ is reported and analyzed. Finally in the last part, we give our conclusions.

II. Methodology

The EGP method is a complex method which has been described in more detail in several previous papers.[1−3,13] However, the method will briefly be explained here. First, a reference system is chosen as the extraction system. This system can be the CO group itself or a molecule which includes the carbonyl in a bonding environment similar to the one that the pseudocarbonyl will be used in. A Hartree−Fock calculation is performed on the reference system, thus yielding a reference Fock operator, $\hat{F}_{ref}$. During the next step, the orbitals required to describe the bonding between the carbonyl and the rest of the reference system are determined, namely, that of the carbon lone pair, 5σ, and the 2π* orbitals (see Figure 1). Then, one has to find the best association of a truncated basis set and the number of electrons kept on C and O in order to reproduce as closely as possible the relevant orbitals previously identified. The reduced system thus obtained is known as the fictitious

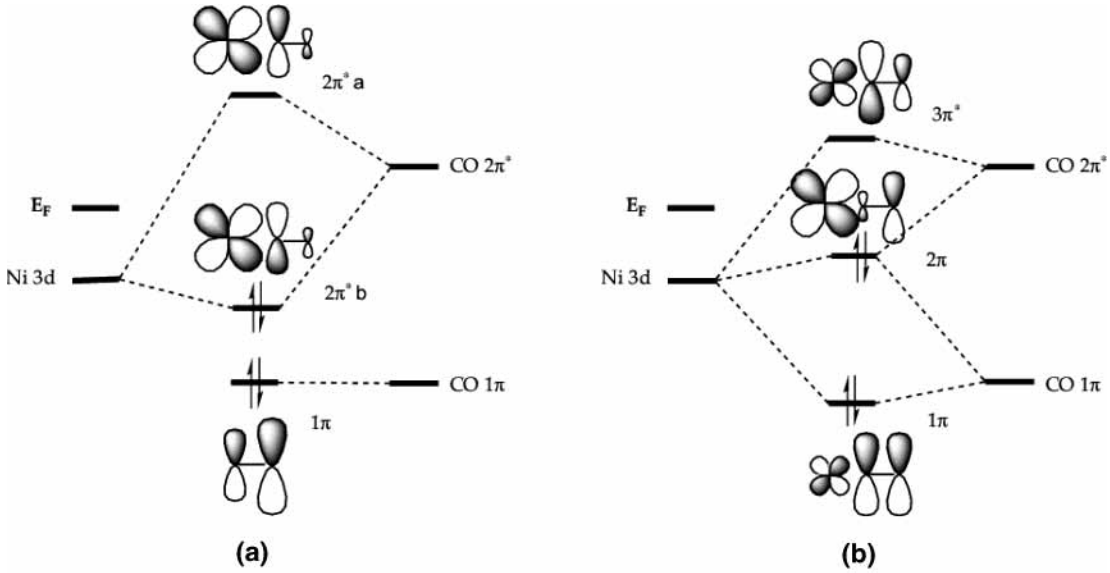

Figure 3. Bonding models of Ni−CO: (a) π system, two-fragment model; (b) π system, three-fragment model (after Nyberg[12]). E_F is the Fermi level.

system. The best combination of nuclear charges and electrons for the carbonyl was found to be $Z_{eff} = 2$ on the pseudocarbon and $Z_{eff} = 0$ on the pseudooxygen, thus yielding an overall number of two electrons for the system.

When the best fictitious system has been found, a calculation is carried out at the Hartree−Fock level in order to obtain the Fock operator $\hat{F}_f$. The orbitals obtained by the diagonalization of the projected $\hat{F}_{ref}$ in the truncated basis set are the so-called molecular valence pseudoorbitals (MVPOs). The MVPOs are designed to be as close as possible to the reference orbitals in energy and shape. The fictive system by itself is unable to fully reproduce the presence of a real carbonyl group. This poor behavior is corrected by the matrix $\mathbf{F}_{EGP}$. This operator is defined as the difference between the two matrix representations $\mathbf{F}_{ref}$ and $\mathbf{F}_f$. $\mathbf{F}_{ref}$ and $\mathbf{F}_f$ are the previously mentioned reference and fictitious operators projected in the basis formed by the MVPOs.

$$\mathbf{F}_{EGP} = \mathbf{F}_{ref} - \mathbf{F}_f \tag{1}$$

At this stage, the matrix $\mathbf{F}_{EGP}$ depends on the basis set of the extraction process and cannot be used for other molecules. In order to have a transferable operator, $\hat{W}_{EGP}$ is defined as a nonlocal monoelectronic operator:

$$\hat{W}_{EGP} = \sum_{n}^{N}\sum_{m}^{N} \alpha_{nm} |g_n\rangle\langle g_m| \tag{2}$$

where $|g_n\rangle$ designates an even-tempered Gaussian functions basis set. The α_{nm} coefficients are determined as proposed by Nicolas and Durand[13] by a least-squares fit in order to minimize the difference between the matrix representations of the two operators:

$$||\mathbf{F}_{EGP} - \mathbf{W}_{EGP}||_{min}^{2} \tag{3}$$

The modeled chemical group is replaced by a reduced number of electrons, a basis set, and an operator $\hat{W}_{EGP}$. The influence of the remaining electrons is described by the operator in association with the basis set. The electronic density on the bond between the active part and the fictitious system being not frozen, the donation−back-donation effect is obtained by including antibonding π*CO virtual orbitals in the set of orbitals to reproduce.

Computational Details. The EGP routines have been included in the Gaussian 98 [14] and Molcas 5 [15] programs. We used basis sets and relativistic atomic pseudopotentials from Stuttgart[16−18] unless otherwise mentioned. For nickel and iron, we did not include f-type basis functions in the calculations. The carbon and oxygen atoms of the pseudocarbonyl, *CO*$^{\#}$, hold nonlocal core pseudopotentials from Toulouse.[19] All geometry optimizations have been performed at the Hartree−Fock level of calculation, using the Gaussian 98 program.[14] To check the validity and the accuracy of the extracted pseudocarbonyls, we systematically performed reference calculations, that is, calculations involving the real carbonyl groups performed at the same level of theory as the EGP calculations. Moreover, it should be recalled that the $\hat{W}_{EGP}$ operator does not contain a distance-dependent term. Thus, those calculations also provide the distance of the interaction between the pseudocarbonyl and the TM. Extraction of the EGP is done at the Hartree−Fock level, but we have shown in previous work[4,5] that use of the EGP can be extended to correlated methods.

III. Results and Discussion

Several attempts at obtaining a satisfying pseudocarbonyl were made. Different processes of extraction were considered, thus yielding a different pseudocarbonyl. As a matter of fact, the definition of the MVPOs and of $\hat{W}_{EGP}$ depends on the reference system, the truncated atomic basis set (size and functions type), and the number of electrons on the pseudocarbon and on the pseudooxygen. The results discussed in this section were obtained using three pseudocarbonyls, *CO*$^{\#i}$. The truncated basis sets as well as the $\hat{W}_{EGP}$ operator are developed on two centers which correspond to C and O atoms. *CO*$^{\#1}$ was extracted from the isolated CO; its basis set consists of one s-type function and two p-type functions on C and two p-type functions on O (see Table 1). We used a smaller basis set for *CO*$^{\#2}$, which is one s- and one p-type function on the pseudooxygen. Moreover, BH_3CO was taken as the reference system. As with *CO*$^{\#1}$, the third EGP was extracted from the isolated CO, but the associated truncated basis set is smaller. We shall see in the following that, although all of the *CO*$^{\#}$'s provide

TABLE 1: Pseudocarbonyl Characteristics[a]

CO#1	*n*	l	exponents	coefficients
C	2	0	0.1217	1.0
		1	0.3139	1.0
		1	0.2117	1.0
O	0	1	0.7500	1.0
		1	0.3004	1.0
CO#2	*n*	l	exponents	coefficients
C	2	0	0.1487	1.0
		1	0.6040	1.0
O	0	1	0.6033	1.0
CO#3	*n*	l	exponents	coefficients
C	2	0	0.1700	1.0
		1	0.8000	1.0
		1	0.5101	1.0
O	0	1	0.8993	1.0

[a] The number of electrons on the pseudoatom is *n*.

TABLE 2: BH_3CO and BF_3CO Geometrical Parameters (Symmetry Point Group: C_{3v})[a,b]

	r_{BC}	r_{CO}	r_{BH}	a_{HBC}
BH_3CO	1.601	1.120	1.201	104.0
$BH_3CO^{\#1}$	1.601*	1.120*	1.228	103.3
$BH_3CO^{\#2}$	1.601*	1.112*	1.202	97.8
$BH_3CO^{\#3}$	1.601*	1.120*	1.218	100.5
	r_{BC}	r_{CO}	r_{BF}	a_{FBC}
BF_3CO	2.810	1.122	1.335	91.4
$BF_3CO^{\#1}$	2.810*	1.120*	1.341	94.0
$BF_3CO^{\#2}$	2.810*	1.112*	1.333	90.1
$BF_3CO^{\#3}$	2.810*	1.120*	1.337	92.6

[a] Bond lengths, *r*, in Å; bond angles, *a*, in deg. [b] Parameters marked with asterisks were frozen during the geometry optimizations.

accurate geometric parameters for the investigated compounds, *CO*#1 fails in the description of the lowest excited states of the organometallic compounds, that is, $Ni(CO)_4$ and $Fe(CO)_5$. However, as in the cyclopentadienyl case,[4] the transferability of EGPs extracted from the isolated species is expected to be better. Thus, we carefully analyzed the difference between the *CO*#1 and *CO*#2 EGPs, and *CO*#3 was designed once the diagnosis was established. Indeed, the $\hat{W}_{EGP}$ operator exhibits a σ component, much more important in *CO*#1 than in *CO*#2 or *CO*#3, which strongly influences both the n_c lone pair and the σ^* virtual orbitals of the pseudo-CO. In the following, the parameters marked with asterisks were frozen during the geometry optimizations, and the distances are given in Å, the angles and dihedral angles in degrees, and the energies in hartrees. The symmetry point group expression is abbreviated as SPG.

A. Geometry Optimizations. *A.1. CO as a Lewis Base: BX_3CO.* Attention was focused on the electronic and geometrical properties of two adducts BH_3CO and BF_3CO (see Table 2 and Figure 4). The deviation of a geometrical parameter *G* with respect to the reference value is calculated using the usual formula:

$$\Delta = \frac{|G_{Ref} - G_{EGP}|}{G_{Ref}} \times 100 \qquad (4)$$

where *G* is the quantity of interest.

The relative error on the bond length B−H due to the use of pseudocarbonyl *CO*#1 is 2.2%, and the relative error for the bond angle HBC is 0.7%. In the case of the complex BF_3CO, the error for the FBC bond angle is 2.8%, whereas the error for the B−F bond length is only 0.4%.

Pseudocarbonyl *CO*#2 extracted from the donor−acceptor compound BH_3CO yielded optimized geometries on BH_3CO and BF_3CO complexes in excellent agreement with the reference calculations. The bond lengths B−X (X = H, F) are overestimated by less than 0.1%, and the bond angles are underestimated by 6.0% for BH_3CO and 1.4% for BF_3CO. As can be seen from Table 1, the *CO*#3 pseudocarbonyl is also accurate.

As far as the energies and shapes of the MOs are concerned, we can see in Figure 4 that there is not an exact superposition between the reference diagram (on the left) and the diagram from the calculation with EGP (on the right). Some MOs, irrelevant for the bonding, do not appear with the EGPs because only the 5σ MO of CO (see Figure 1) is considered. However, there is a substantial error in the energies of the occupied MOs of $BH_3CO^{\#1}$. However, that discrepancy does not affect the geometrical feature of the active part, and at this stage we cannot really distinguish one pseudo-CO from the other.

A.2. Transferability. In the previous section, the accuracy of the pseudo-CO *CO*#1 was tested using the BH_3CO and BF_3CO molecules. However, because we wanted to create a carbonyl able to behave correctly in the vicinity of a TM, we chose several molecules containing TMs to study the behavior of our pseudocarbonyl: $Co(PH_3)_2H(CO)$, $Ni(CO)_4$, and $Fe(CO)_5$.

A.2.a. $Co(PH_3)_2HCO$ (see Table 3). The particularity of this planar molecule is the bending of the phosphine groups. In this complex, the cobalt in the oxidation state +1, Co(I), is d^8. In studying this species, we wanted to test the ability of our pseudopotential to reproduce the correct bending of the two phosphine groups relative to the linear part of the molecule (O−C−Co−H). This test looks mild, but we have checked that inappropriate pseudocarbonyl groups give very bad results such as the collapse of the PH_3 groups onto the pseudocarbonyl during the geometry optimization. The results are encouraging as the angle CCoP is overestimated by 1.6% using *CO*#1 and by 2.6% using *CO*#2. Our pseudopotential thus seems to mimic the σ and π interactions of a real carbonyl. Moreover, the energy gap between the HOMO and the lowest unoccupied molecular orbital (LUMO) is in good agreement with the reference Hartree−Fock calculation: 0.315 72 hartree in $Co(PH_3)_2HCO$ compared to 0.292 84 hartree (corresponding to a relative error of 7.2%) in $Co(PH_3)_2HCO^{\#1}$ and 0.324 90 hartree (corresponding to a relative error of 2.9%) in $Co(PH_3)_2HCO^{\#2}$.

A.2.b. $Ni(CO)_4$ (see Table 4). $Ni(CO)_4$ belongs to the T_d SPG, all the carbonyl groups in $Ni(CO)_4$ being equivalent. Three of the four carbonyl groups of this molecule were replaced by *CO*#'s. With *CO*#1, the C−O bond length of the remaining carbonyl is overestimated by 0.01 Å and the Ni−C bond is 0.024 Å longer whereas the bond angles remain the same. *CO*#2 is more accurate because the C−O bond length of the remaining carbonyl is underestimated by 0.001 Å and the Ni−C bond is 0.004 Å longer whereas the bond angles also remain the same. Although the introduction of three *CO*#'s into the tetracarbonylnickel molecule breaks the T_d symmetry as our pseudocarbonyl groups are not exactly real carbonyls, the angles and dihedrals remain close to the angular T_d symmetry (see Table 4). The results of the geometry optimization of the single CO group are thus in good agreement with the reference calculation. Moreover, the Hartree−Fock energies of the orbitals are fairly well reproduced. We also can note the breaking of the bond orbital degeneracy in $Ni(CO)(CO^{\#})_3$ compared to $Ni(CO)_4$. In the reference calculation, the HOMO is a threefold degenerate orbital at −0.380 63 hartree, whereas with *CO*#1 the threefold

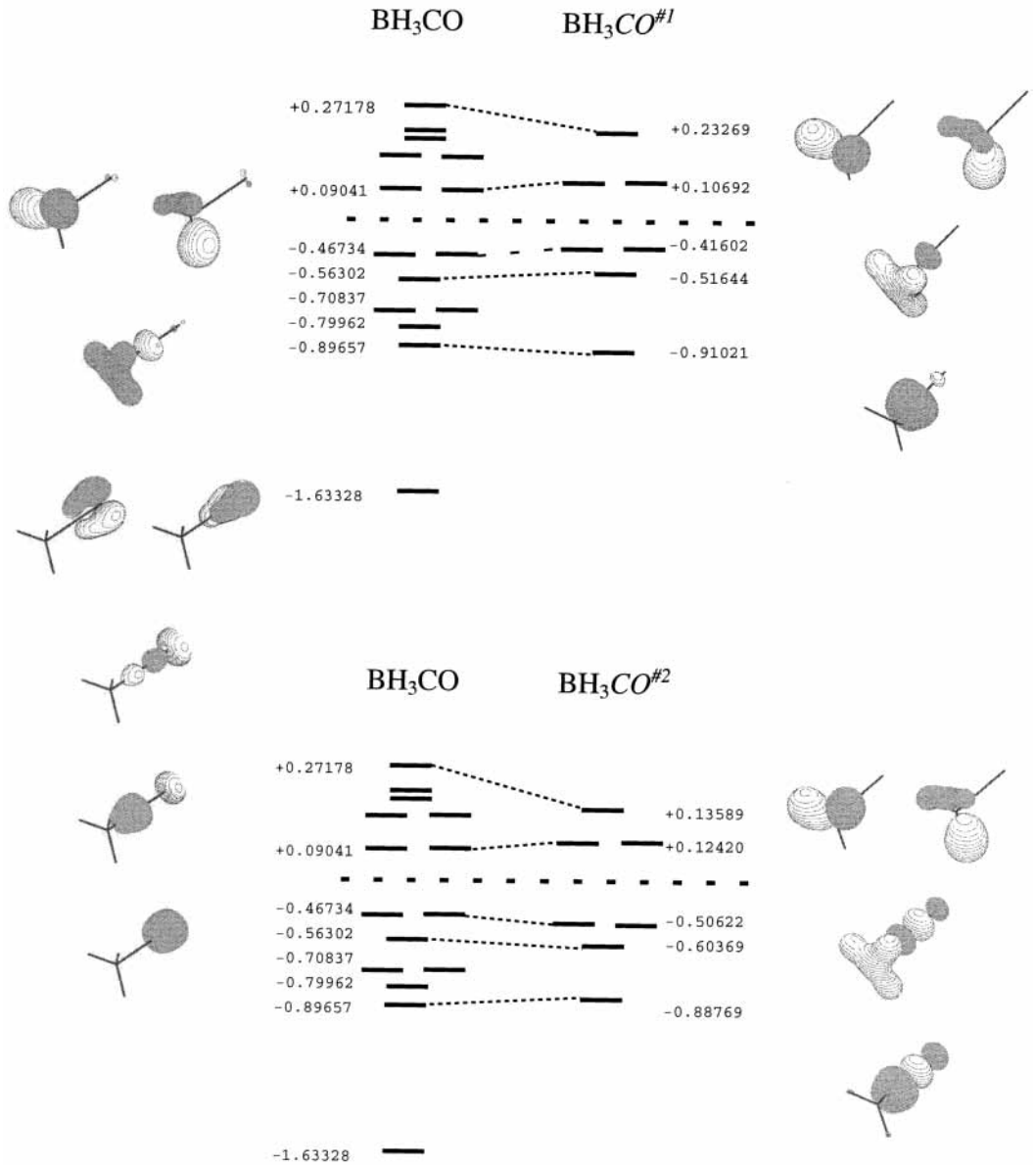

Figure 4. Hartree−Fock energies (in hartrees) of the MOs for BH_3CO, $BH_3CO^{\#1}$, and $BH_3CO^{\#2}$; on the left, the MOs for the reference calculation are shown. Some occupied MOs disappear in the calculations with $CO^{\#1}$ and $CO^{\#2}$. They are MOs from the CO that cannot be reproduced because $CO^{\#1}$ and $CO^{\#2}$ are designed to reproduce only the relevant orbitals for the bonding of CO in interaction with an active part.

degenerate orbital is split into two orbitals at −0.237 89 hartree and one orbital at −0.362 18 hartree. On the one hand, the midpoint of these orbitals constituting the pseudo-HOMO shell is at −0.279 32 hartree. The latter midpoint energy value lies 26.6% lower in energy on a relative basis than the value from the reference calculation. On the other hand, the relative overestimation of the energy midpoint of the pseudo-HOMO using $CO^{\#2}$ compared to the reference HOMO is 9.4%. Indeed, with $CO^{\#2}$ the HOMO shell is split into two energy levels: one orbital at −0.409 91 hartree and one twofold degenerate orbital at −0.425 08 hartree. Although the threefold degeneracy is not expected to remain within $Ni(CO)(CO^{\#})_3$, $CO^{\#1}$ enhances the splitting.

A.2.c. $Fe(CO)_5$ (see Table 5 and Figure 5). $Fe(CO)_5$ belongs to the D_{3h} SPG. In $Fe(CO)_5$, there are two groups of equivalent COs: two axial (or apical) and three equatorial (or basal). Many previous investigations of the iron pentacarbonyl molecule have been performed.[10,20,21] In the current investigation, two kinds of pseudocarbonyl associations were considered. First, two pseudo-COs replaced the two axial carbonyl groups, and second, three pseudo-COs were used in the equatorial positions. Thus, the SPG, D_{3h}, remains unchanged from $Fe(CO)_5$ to $Fe(CO)_3(CO^{\#})_2$ and $Fe(CO)_2(CO^{\#})_3$.

A.2.d. Discussion. Looking at the geometries, $CO^{\#1}$ gives comparable performances when used in the equatorial position or in the axial position. The relative errors for the system $Fe(CO)_3(CO^{\#1})_2$ show that $Fe-C_{eq}$ is shortened by 2.6%, whereas $C-O_{eq}$ is elongated by 0.8%. For the system $Fe(CO)_2(CO^{\#1})_3$, $Fe-C_{ax}$ is shortened by 4.2% and $C-O_{ax}$ is elongated by 0.7%. The shapes of the five highest occupied orbitals of the Hartree−Fock calculations for both $Fe(CO)_5$ and $Fe(CO)_2(CO^{\#1})_3$ are shown in Figure 5. It is obvious from the figure that the energy of the HOMO is overestimated using pseudocarbonyl $CO^{\#1}$ whereas the shapes of the orbitals are comparable.

Similarly, using $CO^{\#2}$ and dealing with $Fe(CO)_5$ geometrical parameters, we compare the relative percent error in the apical and basal positions. In $Fe(CO)_3(CO^{\#2})_2$, the relative error with respect to $Fe-C_{eq}$ is 0.3% and 0.3% with respect to $C-O_{eq}$ and both bonds are elongated in the system with the pseudocarbonyl, whereas in $Fe(CO)_2(CO^{\#2})_3$, the relative error with respect

TABLE 3: Optimized Geometry for $Co(PH_3)_2HCO$ and Optimized Geometry Parameters for $Co(PH_3)_2HCO$, $Co(PH_3)_2HCO^{\#1}$, $Co(PH_3)_2HCO^{\#2}$, and $Co(PH_3)_2HCO^{\#3}$ (Symmetry Point Group: C_2)[a,b]

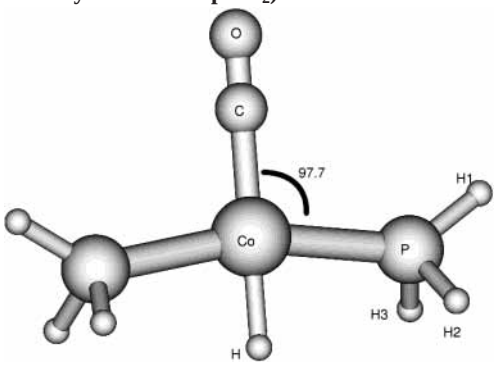

	$Co(PH_3)_2HCO$	$Co(PH_3)_2HCO^{\#1}$	$Co(PH_3)_2HCO^{\#2}$	$Co(PH_3)_2HCO^{\#3}$
Co−C	1.952	1.952*	1.952*	1.952*
Co−P	2.551	2.626	2.495	2.560
Co−H	1.688	1.714	1.680	1.692
C−O	1.126	1.120*	1.112*	1.120*
P−H_1	1.430	1.435	1.427	1.430
P−H_2	1.418	1.421	1.417	1.420
P−H_3	1.418	1.421	1.417	1.420
CCoP	97.7	99.3	95.2	94.3
H_1PCo	138.7	141.6	136.4	135.0
H_2PCo	107.8	107.0	108.5	110.3
H_3PCo	107.8	107.0	108.5	110.4
$HCoPH_1$	180.0	180.0	179.6	179.9
$CoPH_1H_2$	129.7	130.2	129.3	129.9
$CoPH_1H_3$	129.8	130.2	129.3	130.0

[a] Bond lengths in Å; bond angles in deg. [b] Parameters marked with asterisks were frozen during the geometry optimizations.

TABLE 4: $Ni(CO)_3CO^{\#}$ Geometry Optimization (Symmetry Point Group: T_d)[a]

	r_{CO}	r_{NiC}	a_{CNiC}	d_{CNiCC}
$Ni(CO)_4$	1.129	1.873	109.5	120.0
$Ni(CO^{\#1})_3CO$	1.139	1.897	109.5	120.0
$Ni(CO^{\#2})_3CO$	1.124	1.877	109.5	120.0

[a] Bond lengths, *r*, in Å; bond angles, *a* and *d*, in deg.

TABLE 5: $Fe(CO)_x(CO^{\#})_y$ Geometry Optimizations (Symmetry Point Group: D_{3h})[a,b]

		$CO^{\#1}$		$CO^{\#2}$	
	$x = 5$, $y = 0$	$x = 3$, $y = 2$	$x = 2$, $y = 3$	$x = 3$, $y = 2$	$x = 2$, $y = 3$
Fe−C_{ax}	2.039	2.039*	1.954	2.039*	2.035
Fe−C_{eq}	1.855	1.806	1.855*	1.860	1.855*
C−O_{ax}	1.123	1.120*	1.131	1.112*	1.119
C−O_{eq}	1.137	1.146	1.120*	1.134	1.112*

[a] Bond lengths in Å. [b] Parameters marked with asterisks were frozen during the geometry optimizations.

to Fe−C_{ax} is 0.2% and 0.4% with respect to C−O_{ax} but both bonds are shortened.

In conclusion, $CO^{\#1}$ and $CO^{\#2}$ give similarly good performances when used in the basal or apical position, and again, $CO^{\#2}$ appears to be slightly more accurate. In the apical or equatorial position, π and σ responses from $CO^{\#1}$ and $CO^{\#2}$ are not equally solicited (cf. Part I, Uddin and Frenking[10]). Thus, it suggests that $CO^{\#1}$ and $CO^{\#2}$ are able to adapt their behavior to different bonding situations into the framework of TM complexes.

B. Electronic Density. It will be shown in this section that the $CO^{\#1}$ EGP, which appeared to provide less accurate geometries and MO energies, is nevertheless able to properly influence the electronic density on the active part of TM

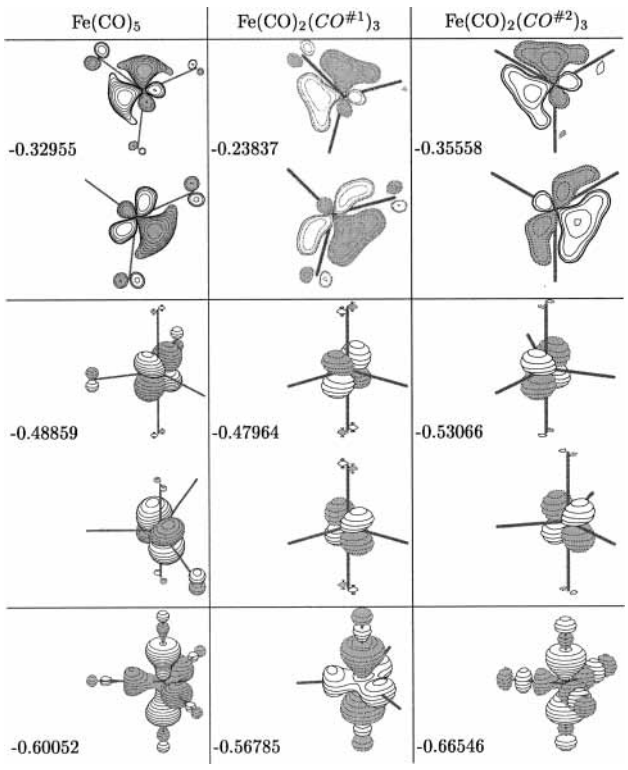

Figure 5. From HOMO to HOMO-2 for $Fe(CO)_5$, $Fe(CO)_2(CO^{\#1})_3$, and $Fe(CO)_2(CO^{\#2})_3$.

complexes. Figure 6 focuses on the iron electronic density calculated from the Hartree−Fock orbitals of $Fe(CO)_5$. In that three-dimensional D_{3h} system, σ and π interactions are coupled; thus, Figure 6 was built by occupying the σ and π orbitals developed simultaneously on the central iron atom and on the ligands. This density is well reproduced using the EGP $CO^{\#1}$

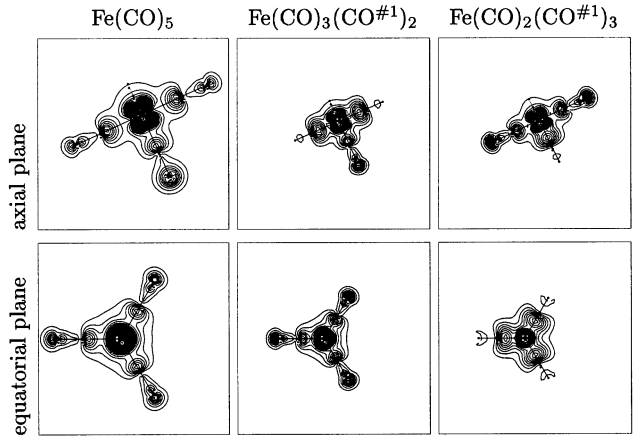

Figure 6. Contour plots of the electronic density calculated from the Hartree−Fock orbitals of $Fe(CO)_5$. The σ and π orbitals developed on the central iron atom and the ligands were used to compute the electronic density. The scale, as well as the space between two isodensity lines, is the same for all the plots.

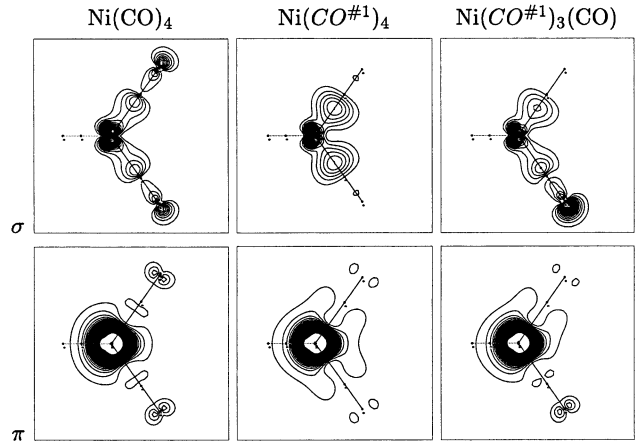

Figure 7. Contour plots of the electronic density calculated from the Kohn−Sham orbitals of $Ni(CO)_4$ in a plane defined by the nickel atom and two carbonyls: (σ) electronic density computed with the four last occupied orbitals "σ_{MC}"; (π) electronic density computed with the five last occupied "π" orbitals. On the figures showing the results for $Ni(CO^{\#1})_3(CO)$, the pseudocarbonyl is up and the real carbonyl is down. The functional is the LDA functional. In the calculations, all of the atoms except the EGP atoms bear a basis set and an atomic core potential from Stuttgart. The scale, as well as the space between two isodensity lines, is the same for all the plots.

in the apical or equatorial positions. As expected, with $CO^{\#1}$ the Fe−$C^{\#}$ bond draws most of the electronic density whereas the reference calculation shows that the density is localized simultaneously on the Fe−C bond, on the C−O bond, and on the oxygen lone pair. However, we can also observe that the substitution of two apical or three equatorial carbonyl ligands by $CO^{\#1}$ does not change significantly the density on the real remaining carbonyl groups. Thus, the density on the active part seems to be well reproduced.

In previous papers,[1−4] we showed the efficiency of EGPs at different levels of calculation of the electronic correlation. Figure 7 presents similar results for the $Ni(CO)_4$ molecule, but the electronic density was calculated here from Kohn−Sham LDA orbitals. Even if in the T_d symmetry the σ and π interactions are coupled, we computed separately the density coming from the last four occupied orbitals "σ_{MC}" and the density coming from the fifth last "π" occupied orbitals. The "π" orbitals are the last T_2 and E shells, which correspond to the metal 3d orbitals. The "σ_{MC}" orbitals correspond to one T_2 shell and the last occupied A_1 shell. The "σ" density on the nickel is well reproduced using the EGP. The Ni−$C^{\#}$ bond draws most of the electronic density whereas the reference calculation reveals that the density of the electrons is localized on the Ni−C bond, the C−O bond, and the oxygen lone pair. In the following, we will focus our attention on the "π" interactions within $Ni(CO)_4$.

For a better understanding at this point, let us discuss the π bonding models of Ni−CO from Figure 3. In the frontier orbital picture (see Figure 3a), which corresponds to the DCD model, one considers only the doubly degenerate π^* interacting orbital on CO and the symmetrically adapted 3d orbitals on Ni. This leads to the formation of two orbitals: one bonding and one antibonding. In this picture, the bonding orbital is occupied and the antibonding MO is unoccupied. Nyberg has shown in ref 12 that if the CO 1π orbital is also included in the bonding scheme (see Figure 3b), three MOs participate in the interaction: the symmetry-adapted 3d of Ni and the 1π and $2\pi^*$ of CO. Linear combinations allow us to form one totally bonding MO, which has an increased character on the C atom and which now contributes to a stronger interaction between this atom and the metal. Then, a second orbital is nonbonding and has a small 2p character on the carbon but a strong metal 3d character and an oxygen 2p character. Higher in energy lies an antibonding MO with a strong CO $2\pi^*$ character.

In light of the previous explanations, the analysis of Figure 7 allows us to say that the pseudocarbonyl behaves in the vicinity of a metal within a two-orbital scheme. Indeed, similarly to the bonding orbital $2\pi^*$, the "π" density is important on the pseudocarbon and a little smaller on the pseudooxygen (see Figure 3a), whereas the reference orbitals show an interaction between the metal and the "true" carbonyls according to a three-fragment model (see Figure 3b): the density is developed on the oxygen and the iron and the carbon contribution to the density is smaller as allowed by the MO 2π from the three-fragment model. The DCD-like description is not enough to obtain the 2π nonbonding orbital of Figure 3b. Our extracted pseudocarbonyl failed by nature to reproduce a three-fragment interaction model. This behavior should be corrected by keeping in the reference orbitals to reproduce the CO 1π orbital. Unfortunately, this is equivalent to keeping quite all from the CO ligand, which is not our goal. Thus, our previous choices (keeping two electrons in the pseudocarbonyl on the carbon, the reduced basis set, the choice of the relevant orbitals, and so forth) impose the $CO^{\#}$ EGP to interact within the DCD model.

As previously said, the "π" density in the reference calculation is weak on the carbon but more developed on the oxygen as within a three-fragment model. Anyway, despite the ability to obtain a correct density on the nickel with $CO^{\#1}$, the pseudocarbonyl enhances the density on the carbon. However, although the pseudocarbonyl behaves within a two-fragment interaction scheme, we have checked in the case of $Ni(CO)(CO^{\#1})_3$ that this does not have a damaging consequence on the active part, that is, Ni(CO). As a matter of fact, we can see in the third column of Figure 7 that the densities on the nickel and on the real CO are comparable to the reference calculation; that is, the interaction scheme between the metal and the carbonyl corresponds to the extended DCD model.

C. Excited States of Tetracarbonylnickel, $Ni(CO)_4$. The aim of the following part of the study was to check the behavior of the $CO^{\#1}$ and $CO^{\#3}$ EGPs in the framework of correlated methods and their ability to reproduce the energy and characteristics of various excited states. The calculations of the excited states of tetracarbonylnickel were carried out using the Molcas 5[15] series of programs for CASSCF and CASPT2 levels. TDDFT

TABLE 6: First Low-Lying Singlet Excitation Energies in TD-LDA for Ni(CO)$_4$, Ni(*CO*$^{\#1}$)$_4$, and Ni(*CO*$^{\#3}$)$_4$, in Electronvolts[a–c]

	states	a^1T_1	a^1E	b^1T_1	a^1T_2	b^1T_2	α^1T_2	α^1E
exptl[d]	T_e				4.6 ± 0.46	5.4 ± 0.54		
theoret[e]	character				56% $t_2 \rightarrow t_2$, 35% $t_2 \rightarrow e$	49% $t_2 \rightarrow e$, 23% $t_2 \rightarrow t_2$		
	T_e	4.36	4.60	4.62	4.70 (0.006)	4.82 (0.099)		
Ni(CO)$_4$	character	89% $t_2 \rightarrow t_2$	100% $t_2 \rightarrow t_2$	100% $t_2 \rightarrow e$	61% $t_2 \rightarrow t_2$, 39% $t_2 \rightarrow t_1$	45% $t_2 \rightarrow e$, 28% $t_2 \rightarrow t_1$, 27% $t_2 \rightarrow t_2$		
	T_e	4.32	4.55	4.57	4.65	4.79		
Ni(*CO*$^{\#1}$)$_4$	character	72% $t_2 \rightarrow t_2$	84% $t_2 \rightarrow t_2$	69% $t_2 \rightarrow e$, 31% $t_2 \rightarrow t_2$	74% $t_2 \rightarrow t_2$	88% $t_2 \rightarrow e$		
	T_e	4.30	4.48	4.38	4.55	4.67	*3.25*	*4.42*
Ni(*CO*$^{\#3}$)$_4$	T_e	4.20	4.52	4.34	4.48	4.86		

[a] Oscillator strengths are indicated in parentheses. [b] The characters of the transitions for Ni(*CO*$^{\#3}$)$_4$ are similar to the one for Ni(*CO*$^{\#1}$)$_4$. [c] In the two last columns (in italics), the excited states are built on the unphysical HOMO in Ni(*CO*$^{\#1}$)$_4$. [d] Gas-phase experiment, ref 29. [e] Data from ref 24.

calculations were carried out with Gaussian 98,[14] along with the LDA functional. Although the TDDFT methodology is still under development,[22,23] it is starting to be widely used and provides a simple way to investigate the lowest excited states of organic or inorganic molecules. Thus, it is considered in this work to be an efficient tool for evaluating the behavior of the EGPs when dealing with excited states.

C.1. TDDFT Level of Theory (see Table 6). According to the work of van Gisbergen et al.[24] and our calculations, the LUMO of Ni(CO)$_4$ exhibits the expected threefold shell of t_2 symmetry. Unfortunately, the LUMO for Ni(*CO*$^{\#1}$)$_4$ is an orbital with a_1 symmetry which lies higher up in the spectrum in the reference calculation. The introduction of this a_1 orbital is due to the use of our *CO*$^{\#1}$ EGP. This artifact leads to excited states without physical meaning because they are built on this a_1 LUMO. Moreover, we obtain a state order slightly different from the reference calculations where only the states a^1E and b^1T_1 are interchanged. This probably results from the fact that the state a^1E in Ni(*CO*$^{\#1}$)$_4$ is slightly affected by an excitation toward the a_1 nonphysical LUMO. Despite the fact that the energies obtained using *CO*$^{\#1}$ are slightly too low, the character description of the states shows that the correct states have been obtained.

In a method which uses directly all of the virtual MOs, *CO*$^{\#1}$ could lead to artifacts for the determination of excited states. However, the aforementioned problem vanished when using methods such as CASSCF because we chose the MOs in the active space.

C.2. Ab Initio Level of Theory (See Table 7). CASSCF and CASPT2 calculations were performed for tetrahedral Ni(*CO*$^{\#1}$)$_4$ using D_2 symmetry and experimental values for the Ni−C distances ($r_{NiC} = 1.838$ Å). For comparison, the CASSCF active space was chosen to be the same as that used by Pierloot et al.;[25] several other groups have performed excited state calculations with ab initio methods on Ni(CO)$_4$ (see Nooijen et al.[26,27] and Nakai et al.[28]). The orbital description for all electrons in the Ni(CO)$_4$ system was used, although it must be recalled that we are dealing here with fewer orbitals because of the four *CO*$^{\#1}$ which are models for the real carbonyls and because of the effective core potential on each atom. To prevent the mixing of MOs originating from different representations in T_d, our CASSCF steps contain symmetry restrictions. Ni(CO)$_4$ is a d^{10} system, with 3d electrons occupying the 2e and $9t_2$ shells. Nondynamical correlation effects in the system are mainly taken into account by including the (2,3)e and (9,10)t_2 shells in the CASSCF active space. Moreover, to provide an accurate description of the relevant excited states, the $2t_1$ shell is included in the active space as well. All excited states are calculated using a 13-orbital active space with 10 electrons. CASPT2 includes with a second-order perturbation approach the remaining correlation effects. Finally, the oscillator strengths are calculated at the CASSCF level for the symmetry- and spin-allowed transitions. Table 7 shows the results from various methods with respect to the first low-lying singlets of the tetracarbonylnickel compound. The energies show a wide range of values. The results obtained using *CO*$^{\#1}$ (see Table 7) yielded a T_1 state as the first low-lying singlet (4.23 eV) which at the CASPT2 level is close in energy to an A_1 state (4.24 eV), followed by a T_2 state (4.71 eV). The state a^1T_2 found at 4.71 eV using CASPT2 is in good agreement with the observed spectrum[29] considering the 10% relative error in the experimental values. Given the great variation in the results shown in Table 7, the values obtained with *CO*$^{\#1}$ are clearly acceptable for the physical states, that is, those which are not described by an excitation toward the a_1 LUMO. The choice of the atomic pseudopotential type influences the results. The results at the CIM (configuration interaction including only the monoexcitations) level of calculation for Ni(CO)$_4$ using (a) basis sets and associated atomic pseudopotentials from Stuttgart[16–18] and (b) basis sets and associated pseudopotentials from Seijo et al.[30] show that under (a) conditions the first T_1 singlet state in CIM is at 4.73 eV and under (b) conditions it is at 4.50 eV. Similarly, the first T_2 singlet state in CIM lies at 5.26 eV and at 5.02 eV under (b) conditions. We do not pretend to get better accuracy than the incertitude which the choice of various atomic pseudopotentials introduces, that is, about 0.2 eV. Thus, considering that the results with

TABLE 7: First Low-Lying Singlet Excitation Energies for Ni(CO)$_4$: Results for Various Methods and First Low-Lying Singlet Excitation Energies in CASSCF and CASPT2 for Ni(*CO*$^{\#1}$)$_4$, in Electronvolts[a]

state	a^1T_1	a^1A_1	a^1T_2
	Ni(CO)$_4$		
exptl[b]	4.6 ± 0.46		
EOM-CCSD[c]	4.61	5.45	4.93
STEOM-CCSD[c]	4.29	5.07	4.60 (0.0042)
ext-STEOM[c]	3.92	4.75	4.24
CASSCF[d]	7.15	9.12	7.49 (0.29)
CASPT2[d]	4.46	4.37	4.76 (0.29)
CASPT2(c−v)[d]	4.04	3.72	4.34 (0.29)
SAC−CI[e]	4.53	5.41	4.79 (0.0023)
TD-LDA[f]	4.36		4.70 (0.006)
	Ni(*CO*$^{\#1}$)$_4$		
CASSCF	4.58	5.07	5.20 (0.0914)
CASPT2	4.23	4.24	4.71 (0.0914)

[a] Oscillator strengths are indicated in parentheses. [b] Gas-phase experiment, ref 29. [c] Ab initio data from refs 26 and 27. [d] Ab initio data from ref 25. [e] Ab initio data from ref 28. [f] Data from ref 24.

our $CO^{\#1}$ are satisfactory and that the reduction of CPU time and memory space induced by the use of the EGP methodology means that we can extend our CASSCF active space, our method will result in a great improvement in the accurate determination of $Ni(CO)_4$ excited states. However, this EGP introduces nonphysical states among the low-lying singlet states. There is a need for building an EGP able to suitably position the lowest virtual σ^* orbitals of CO in the MO spectrum.

C.3. Design of an Improved $CO^{\#}$ EGP. Because the calculated spectrum for $Ni(CO)_4$ at the TD-LDA level using $CO^{\#1}$ exhibited artifacts, we decided to build another pseudocarbonyl $CO^{\#3}$ from the isolated carbonyl molecule as we did for $CO^{\#1}$. Some considerations concerning the extraction process were given at the beginning of this section. We expect that they will lead to a better description of the virtual spectrum of $Ni(CO)_4$. Therefore, we calculated the spectrum of $Ni(CO^{\#3})_4$ at the LDA level of theory. The virtual orbital with a_1 symmetry recovers a level in agreement with the reference spectrum. At this stage, we want to validate $CO^{\#3}$ according to geometrical optimization. We optimized $Co(PH_3)_2HCO^{\#3}$, and the results are slightly better than those obtained with $CO^{\#1}$ (see Table 3). However, $CO^{\#1}$, $CO^{\#2}$, and $CO^{\#3}$ (i.e., for each $CO^{\#}$, a truncated basis set and its corresponding EGP operator) can be considered to give similar results according to the geometries. In other words, there are not unique and unequivocal choices with which to build a $CO^{\#}$; all pseudo-COs show the same accuracy when only the ground state is considered (choice of the truncated basis set, choice of the Gaussian functions of the EGP operator, and so forth). Moreover, $CO^{\#1}$, $CO^{\#2}$, and $CO^{\#3}$ are built to make the σ lone pair of the carbon and the two π virtual orbitals important for the back-bonding, but we did not work on the rest of the virtual spectrum. After the test on the geometry, we calculate in TD-LDA the first low-lying singlets of $Ni(CO^{\#3})_4$ (see Table 6). The results obtained for $CO^{\#3}$, qualitatively similar to $CO^{\#1}$, do not exhibit undesired low-lying states. We are not looking for absolute spectroscopic accuracy, but we wish to predict at least semiquantitatively visible and dipole-forbidden transitions within the 0.2 eV accuracy. Moreover, when we go through the results from ab inito to CIM to TDDFT and CASPT2, the transition energies using $CO^{\#}$'s are in the same range as those with real carbonyl ligands (see Tables 6 and 7). To conclude, we could design $CO^{\#3}$ in order to calculate excited states. $CO^{\#3}$ enables us to have a nice virtual spectrum for $Ni(CO)_4$ without deteriorating the efficiency geometry optimizations.

IV. Concluding Remarks

Modeling a carbonyl ligand for TM complexes has been a challenge for the EGP methodology. The building of MVPOs of the reduced system is now straightforward, and the robustness of the $\hat{W}_{EGP}$ operator is assessed for the purpose of geometry optimization. However, the problems we encountered for the description of excited states provide a motivation for elaborating an extraction process more formally grounded when dealing with virtual MOs. Such work is in progress in the spirit of effective Hamiltonian methodologies. Nevertheless, the results obtained for this extreme case show much promise for further investigations. Our next aim is to model some of the phosphine ligands, which are very important and common for the chemistry of TMs. The classification of the ligands by decreasing π acceptor power is as follows:

$$NO > CO \approx RNC \approx PF_3 > PCl_3 > PCl_2(OR) > PCl_2R > PBr_2R > PCl(OR)_2 > PClR_2 > P(OR)_3 > PR_3 \approx SR_2 > RCN > RNH_2 \approx OR_2$$

The π acid character of a carbonyl ligand is greater than the π acidity of any of the phosphine ligands. Thus, we could expect that phosphines correspond better to the separability criteria required by the EGP method. Therefore, the results can be expected to be more accurate than those obtained for the carbonyl ligand model. Furthermore, we would like to identify the irrelevant information in the framework of an apparently complex problem. This goal means more than the reduction of ab initio calculations. Moreover, this identification should begin upstream of the method. Thus, we propose to perform systematic wave function analysis (such as AIM[31,32] or NBO[33] analysis) and energy decomposition analysis (such as ETS[9]) in order to gain deeper insight into the nature of the bonding of the specific ligand.

Acknowledgment. The authors acknowledge computer time support from the CALMIP (CALcul en MIdi-Pyrénées), Project p0307.

References and Notes

(1) Alary, F.; Poteau, R.; Heully, J.-L.; Barthelat, J.-C.; Daudey, J.-P. *Theor. Chem. Acc.* **2000**, *104*, 174−178.

(2) Poteau, R.; Ortega, I.; Alary, F.; Solis, A. R.; Barthelat, J.-C.; Daudey, J.-P. *J. Phys. Chem. A* **2001**, *105*, 198−205.

(3) Poteau, R.; Alary, F.; Makarim, H. A. E.; Heully, J.-L.; Barthelat, J.-C.; Daudey, J.-P. *J. Phys. Chem. A* **2001**, *105*, 206−214.

(4) Alary, F.; Heully, J.-L.; Poteau, R.; Maron, L.; Trinquier, G.; Daudey, J.-P. *J. Am. Chem. Soc.* **2003**, *125*, 11051−11061.

(5) Maron, L.; Perrin, L.; Eisenstein, O.; Andersen, R. A. *J. Am. Chem. Soc.* **2002**, *124* (20), 5614.

(6) Dewar, M. J. S. *Bull. Soc. Chim. Fr.* **1951**, *18*, C79.

(7) Chatt, J.; Duncanson, L. A. *J. Chem. Soc.* **1953**, 2929.

(8) Blyholder, G. *J. Chem. Phys.* **1964**, *68*, 2772.

(9) Ziegler, T.; Rauk, A. *Theor. Chim. Acta* **1977**, *46*, 1−10.

(10) Uddin, J.; Frenking, G. *J. Am. Chem. Soc.* **2001**, *123* (8), 1683−1693.

(11) Bauschlicher, C. W. J.; Bagus, P. S. *J. Chem. Phys.* **1984**, *81* (12), 5889−5898.

(12) Nyberg, M. Probing Adsorbate−Surface Chemical Bonds Using Ab Initio Techniques Combined with X-ray Spectroscopy. M.S. Thesis, Stockholm University, Stockholm, Sweden, 2000.

(13) Nicolas, G.; Durand, P. *J. Chem. Phys.* **1979**, *72* (1), 453−463.

(14) Frisch, M. J.; Trucks, G. W.; Schlegel, H. B.; Scuseria, G. E.; Robb, M. A.; Cheeseman, J. R.; Zakrzewski, V. G.; Montgomery, J. A., Jr.; Stratmann, R. E.; Burant, J. C.; Dapprich, S.; Millam, J. M.; Daniels, A. D.; Kudin, K. N.; Strain, M. C.; Farkas, O.; Tomasi, J.; Barone, V.; Cossi, M.; Cammi, R.; Mennucci, B.; Pomelli, C.; Adamo, C.; Clifford, S.; Ochterski, J.; Petersson, G. A.; Ayala, P. Y.; Cui, Q.; Morokuma, K.; Malick, D. K.; Rabuck, A. D.; Raghavachari, K.; Foresman, J. B.; Cioslowski, J.; Ortiz, J. V.; Stefanov, B. B.; Liu, G.; Liashenko, A.; Piskorz, P.; Komaromi, I.; Gomperts, R.; Martin, R. L.; Fox, D. J.; Keith, T.; Al-Laham, M. A.; Peng, C. Y.; Nanayakkara, A.; Gonzalez, C.; Challacombe, M.; Gill, P. M. W.; Johnson, B. G.; Chen, W.; Wong, M. W.; Andres, J. L.; Head-Gordon, M.; Replogle, E. S.; Pople, J. A. *Gaussian 98*, revision a.1; Gaussian, Inc.: Pittsburgh, PA, 1998.

(15) Andersson, K.; Barysz, M.; Bernhardsson, A.; Blomberg, M. R. A.; Cooper, D. L.; Fleig, T.; Fülscher, M. P.; de Graaf, C.; Hess, B. A.; Karlström, G.; Lindh, R.; Malmqvist, P.-Å.; Neogrády, P.; Olsen, J.; Roos, B. O.; Schimmelpfennig, B.; Schütz, M.; Seijo, L.; Serrano-Andrés, L.; Siegbahn, P. E. M.; Stålring, J.; Thorsteinsson, T.; Veryazov, V.; Widmark, P.-O. *Molcas*, version 5, Lund University: Sweden, 2000.

(16) Dolg, M.; Wedig, U.; Stoll, H.; Preuss, H. *J. Chem. Phys.* **1987**, *86*, 866.

(17) von Szentpaly, L.; Fuentealba, P.; Preuss, H.; Stoll, H. *Chem. Phys. Lett.* **1982**, *93*, 555.

(18) Fuentealba, P.; Stoll, H.; von Szentpaly, L.; Schwerdtfeger, P.; Preuss, H. *J. Phys. Chem. B* **1983**, *16*, 1323.

(19) Durand, P.; Barthelat, J.-C. *Theor. Chim. Acta* **1975**, *38*, 283−302.

(20) Leadbeater, N. *Coord. Chem. Rev.* **1999**, *188*, 35−70.

(21) Bauschlicher, C. W. J.; Bagus, P. S. *J. Chem. Phys.* **1984**, *81* (12), 5889−5898.
(22) Tozer, D. J.; Amos, R. D.; Handy, N. C.; Roos, B. O.; Serrano-Andres, L. *Mol. Phys.* **1999**, *97* (7), 859−868.
(23) Casida, M. E.; Jamorski, C.; Casida, K. C.; Salahub, D. R. *J. Chem. Phys.* **1998**, *108* (11), 4439−4449.
(24) van Gisbergen, S. J.; Groeneveld, J. A.; Rosa, A.; Snijders, J. G.; Baerends, E. J. *J. Phys. Chem. A* **1999**, *103* (34), 6835−6844.
(25) Pierloot, K.; Tsokos, E.; Vanquickenborne, L. G. *J. Phys. Chem.* **1996**, *100* (41), 16545−16550.
(26) Nooijen, M. *J. Phys. Chem.* **1999**, *111* (24), 10815−10826.
(27) Nooijen, M.; Lotrich, V. *J. Chem. Phys.* **2000**, *113* (2), 494−507.
(28) Nakai, H.; Ohmori, Y.; Nakatsuji, H. *J. Chem. Phys.* **1991**, *95*, 8287.
(29) Kotzian, M.; Roesch, N.; Schroeder, H.; Zerner, M. C. *J. Am. Chem. Soc.* **1989**, *111* (20), 7687−7696.
(30) Rakowitz, F.; Marian, C. M.; Seijo, L. *J. Chem. Phys.* **1999**, *111* (23), 10436.
(31) Bader, R. F. W. *Chem. Rev.* **1991**, *91*, 893.
(32) Bader, R. F. W. *Atoms in Molecules*; Clarendon Press: Oxford, 1990.
(33) Reed, A. E.; Curtiss, L. A.; Weinhold, F. *Chem. Rev.* **1988**, *88* (6), 899−926.